TITLE: Human Amniocytes Are Receptive to Chemically Induced Reprogramming to Pluripotency

AUTHORS: Hawkins, K. E., Moschidou, D., Faccenda, D., Wruck, W., Martin-Trujillo, A., Hau, K.-L., Ranzoni, A. M., Sanchez-Freire, V., Tommasini, F., Eaton, S., De Coppi, P., Monk, D., Campanella, M., Thrasher, A. J., Adjaye, J. and Guillot, P. V.

JOURNAL: Molecular Therapy

PUBLISHER: Elsevier

PUBLICATION DATE: February 2017

DOI: 10.1016/j.ymthe.2016.11.014

Human amniocytes are receptive to chemically-induced reprogramming to pluripotency.

Kate E. Hawkins[1], Dafni Moschidou[1], Danilo Faccenda[2], Wasco Wruck[3], Alex Martin-Trujillo[4], Kwan-Leong Hau[1,5], Anna Maria Ranzoni[1], Veronica Sanchez-Freire[6], Fabio Tommasini[1,7], Simon Eaton[6], Paolo De Coppi[6], David Monk[3], Michelangelo Campanella[2,8], Adrian J. Thrasher[7], James Adjaye[3] and Pascale V Guillot[1].

[1] University College London, Institute for Women's Health, Maternal and Fetal Medicine Department, London, United Kingdom.
[2] The Royal Veterinary College, Department of Comparative Biomedical Sciences, London, United Kingdom.
[3] Institute for Stem Cell Research and Regenerative Medicine, Heinrich Heine University Dusseldorf, Dusseldorf, Germany.
[4] Imprinting and Cancer Group, Cancer Epigenetic and Biology Program, Bellvitge Institute for Biomedical Research (IDIBELL), Hospital Duran i Reynals, Barcelona, Spain.
[5] Imperial College London, National Heart and Lung Institute, London, United Kingdom.
[6] Stanford University, Departments of Medicine and Radiology, Stanford CA, USA.
[7] University College London, Institute for Child Health, London, United Kingdom.
[8] University College London, Consortium for Mitochondrial Research, London, United Kingdom.

*** Corresponding author**: Pascale V. Guillot University College London, Institute for Women's Health, Department of Maternal and Fetal Medicine, 86-96 Chenies Mews, London, WC1N 1EH, United Kingdom. Email: p.guillot@ucl.ac.uk, Phone: +44 (0)207 242 9789, Fax: +44 (0)207 404 618

Abstract

Restoring pluripotency using chemical compounds alone would be a major step forward in developing clinical grade pluripotent stem cells, but this has not yet been reported in human cells. We previously demonstrated that human amniocytes cultivated with valproic acid (VPA_AFS cells) acquired functional pluripotency whilst remaining distinct from embryonic stem cells (hESCs), questioning the relationship between modulation of cell fate and molecular regulation of the pluripotency network. Here, we used single cell analysis and functional assays to reveal that VPA treatment resulted in a homogenous population of self-renewing non-transformed cells that fulfil hallmarks of pluripotency, i.e. a short G1 phase, a dependence on glycolytic metabolism, expression of epigenetic modifications on histones 3 and 4, and reactivation of endogenous OCT4 and downstream targets albeit at a lower level than that observed in hESCs. Mechanistic insights into the process of VPA-induced reprogramming revealed that it was dependent on OCT4 promoter activation, which was achieved independently of the P13K/AKT/mTOR pathway or GSK3β inhibition, but was concomitant with the presence of acetylated histones H3K9 and H3K56, which promote pluripotency. Our data identify for the first time the pluripotent transcriptional and molecular signature and metabolic status of human chemically-induced pluripotent stem cells.

Introduction

The reprogramming of somatic cells to pluripotency was originally pioneered by forced expression of transcription factors (TFs) using retroviral transduction[1]. Alternative strategies have since been developed to minimise the number of TFs used[2] and to produce footprint-free induced pluripotent stem cells (iPSCs) without genomic alterations[3, 4]. Ultimately, the complete replacement of ectopically expressed TFs by chemical compounds (CiPSCs) would hold much promise for the use of iPSCs derivates in regenerative medicine. To date, this has not yet been achieved in human cells. The two major barriers to chemical-based reprogramming are (1) to establish a cocktail of mutliple epigenetic modifiers and inhibitors that would reactivate the endogenous pluripotent network, and (2) to find a target cell source which chromatin configuration is most permissive to such chemical treatments.

Paving the way for the generation of human CiPSCs, iPSCs have been generated from human fetal stem cells by ectopically expressing OCT4 alone[5,6]. This suggests that stem cells present during early fetal development may be more amenable to reprogramming than terminally differentiated cells found in adult tissues. However, the accessibility of the cells is of paramount importance for developing autologous CiPSCs. Similar to other fetal mesenchymal stem cells (MSCs)[7], human amniocytes (amniotic fluid stem cells, i.e. AFS cells) are multipotent and differentiate readily into bone, fat and cartilage. They are not tumorigenic, present a low immunogenicity[8], and maintain their phenotype and karyotype after cryopreservation and *in vitro* expansion, making them ideal candidates for translational use[9]. AFS cells are characterised by the expression of the standard MSC surface markers CD73, CD90 and CD105[10,11],

along with SSEA4 and CD177. Whilst they are not pluripotent and do not express SOX2, NANOG, or OCT4A[12-14,9] (the only isoform with a pivotal role in self-renewal and pluripotency[15]), they present a higher degree of plasticity compared to adult MSCs, are more rapidly and efficiently reprogramed to pluripotency[16-18], and are amenable to reprogramming using only OCT4[6].

We previously reported in two independent studies that human amniocytes cultivated on Matrigel in feeder-free hES cell conditions with the histone deacetylase inhibitor valproic acid (VPA, 2-propyl pentanoic acid)[19], i.e. VPA_AFS cells, gained the capacity to form embryoid bodies (EBs) containing cells that expressed ectoderm (NESTIN, PAX6), primitive endoderm (BMP4), endoderm (CK3, CK19) and mesendoderm (GATA6) markers[11-13]. When injected subcutaneously into immunodeficient mice, VPA_AFS cells formed well-differentiated teratomas within 4-6 weeks, which contained derivatives of all three germ layers, as evidenced by immunostaining, i.e. ectoderm (β-Tubulin, NESTIN, NR1), mesoderm (α-ACTININ), and endoderm cells (SOX17, HNF-3β, AFP)[11-13]. After 6-8 weeks of *in vitro* expansion in ESC conditions, VPA_AFS cells (but not AFS cells) were capable of differentiating towards the definitive endoderm (CXCR4, SOX17$^+$ and HNF-3β$^+$, immunostaining) when cultured in serum-free conditions in the presence of Activin-A. When cultured in hepatocyte permissive medium, VPA_AFS cells (but not AFS cells) also differentiated into ALBUMIN$^+$ AFP$^+$ cells which produced urea. These results show that compared to AFS cells, VPA_AFS cells have a higher developmental potential, and suggest that they have acquired functional pluripotency[11-13].

However, genome-wide transcriptome analysis of the entire VPA_AFS cell population revealed that, despite being clearly separated from AFS cells, they remain different from hES cells[6-8]. This questions the relationship between cell potency and molecular

state of the pluripotent network. To address this gap in knowledge, we used single cell analysis and a range of functional assays to comprehensively characterise VPA_AFS cells and understand how they relate to hES cells. We uncover for the first time that human amniocytes cultured in hESC conditions and treated with VPA aquired some molecular, epigenetic and phenotypic features of pluripotency, and that the effect of VPA is OCT4A-dependent. We observed a reactivation of endogenous OCT4 and downstream targets in all individual VPA_AFS cells (albeit levels were not as high as those found in hESCs), resulting in a short cell cycle G1 phase and a dependence on glycolytic metabolism. Together, these data indicate that human amniocytes are a candidate cell source for developing chemical-based protocols to revert human cells to the naïve pluripotent state, and to produce autologous clinical-grade pluripotent stem cells.

RESULTS

VPA_AFS cells aquired functional pluripotency but are molecularly different from hES cells

The present study characterised the molecular state of the same three AFS cell samples which previously formed EBs and teratomas[11-13]. We first used the colony formation in soft agar assay to determine that VPA treatment did not induce the transformation of VPA_AFS cells, as evidenced by their inability to show anchorage-independent growth (**Supplementary Figure 1a**).

Flow cytometry showed that the pluripotency-associated cell surface markers TRA-1-

60, TRA-1-81 and SSEA3, and the nuclear TFs NANOG and OCT4A were expressed in hES cells and absent in AFS cells but expressed in VPA_AFS cells, albeit plots showed overlapping tails with the isotype control for some of these proteins, which indicates the population is heterogeneous (**Figure 1a**). However, scatter plot analysis of the whole population transcriptome showed that VPA_AFS cells were molecularly distinct from hES cells (r = 0.84), with the heatmap of pluripotency-associated genes showing lower expression levels in VPA_AFS cells (**Figure 1b**).

VPA_AFS cells gained *OCT4* and *NANOG* expression with high efficiency

As the results presented above were obtained on the whole population, it is possible that the low correlation (r = 0.84) between VPA_AFS cells and hES cells was due to the heterogeneity of the AFS cell population to reactivate endogenous OCT4 and NANOG. To measure the efficiency of the VPA treatment in AFS cells, we introduced OCT4-GFP (Cellomics Technology # PLV-10050-50) or NANOG-GFP vectors (Plasmid 21321: PL-SIN-Nanog-EGFP, Addgene) in order to detect OCT4 and NANOG expression. All three AFS cell samples transfected with NANOG-GFP and OCT4-GFP and cultured in D10 (DMEM + 10% FBS) were negative for cell surface marker TRA-1-60, which is considered one of the best markers for human pluripotent stem cells[21], but gained TRA-1-60 expression upon VPA treatment **(Figure 2).** TRA-1-60^{+} cells were then single cell sorted into four 96-well plates coated with Matrigel (total of 384 cells analysed for each condition) and placed in an incubator for an additional 28 days, during which GFP expression was monitored 7, 14 and 28 days later using an optical plate reader **(Figure 2a)**. TRA-1-60 expression was maintained

homogeneously in almost all cells (>85% of the cell population) over 28 days. Optical analysis of the plates indicated that the cells formed clones of variable size all expressing GFP, indicating (1) that VPA treatment reactivated OCT4 and NANOG expression, (2) that the acquired phenotype (expression of TRA-1-60, OCT4 and NANOG) was stable, and (3) that VPA treatment was highly efficient (**Figure 2b, 2c**). We validated the use of OCT4-GFP lentiviral reporter approach by showing that GFP expression correlates with the pattern of OCT4 expression demonstrated by immunostaining (**Figure 2d**).

VPA_AFS cells changed cell size, presented a short G1 phase and switched their metabolism towards glycolysis

As previously demonstrated, VPA_AFS cells grew as compact colonies (**Figure 3a**), and a flow scatter analysis showed that the size of individual VPA_AFS cells was in average smaller that the size of the cells from the AFS cell population, i.e. forward scatter (FSC) median 278 vs. 809 (10000 cells analysed for each conditions) (**Figure 3b**), although this observation alone does not indicate that the cells are pluripotent.

Propidium iodine staining and flow cytometry analysis of the cell cycle showed that AFS cells predominantly presented a distribution typical of diploid DNA content in the G1 phase of the cell cycle, indicating that the cells were in a pre-replicative state. In contrast, VPA_AFS cells showed a shortened G1 phase and a longer S phase (synthesis of DNA) for each cycle, which resulted in a shorter G1/S-phase ratio, a feature associated with maintenance of the undifferentiated state in pluripotent stem cells[22-24], with hES cells demosntrating a similar pattern (**Figure 3c**).

To determine the metabolic phenotype of VPA_AFS cells, ATP levels were monitored dynamically by fluorescence (see Methods). The resistance to oligomycin treatment is indicative of a metabolic switch towards glycolysis. Mg provides an index of changing ATP concentration and is an indirect read-out for ATP depletion. The drop in ATP is thus proportional to the increase in fluorescence. The more prominent is the OXPHOS the greater will be the rise in fluorescence consequently plotted. The opposite occurs when OXPHOS is scares. Living AFS cells and VPA_AFS cells (1 million cells per sample, three samples tested for each group) positively loaded with the MgGreen dye were challenged with the chemical inhibitor of the Complex V oligomycin, and changes in fluorescence were recorded and quantified. In AFS cells, but not in VPA_AFS cells, we detected a clear and sustained increase in fluorescence within minutes ($P<0.05$), with the graph and chart plotting in corresponding to an increase in depletion (**Figure 3d**). A greater contribution of mitochondria to energy metabolism and an oxidative phenotype could account for this increase in fluorescence intensity in AFS cells.

We next examined mitochondrial oxidative metabolism using carbon dioxide ($^{13}CO_2$) production as a marker, as ^{13}C-pyruvate is produced by glycolysis and then oxidized in the mitochondria to yield $^{13}CO_2$. After 4 h incubation with [U-^{13}C]-D-glucose, $^{13}CO_2$ released in the culture medium and in the sealed culture flasks air was measured. Compared to AFS cells (undifferentiated and differentiated down the osteoblast lineage), VPA_AFS cells demonstrated a significantly ($P<0.05$) lower production of $^{13}CO_2$ ($P<0.05$), which is indicative of a lower oxidative metabolism, albeit levels did not reach those of hES cells (**Figure 3e**).

Together, these data indicated that VPA_AFS cells presented a higher dependance on glycolysis over OXPHOS, a feature associated with the pluripotent state in human

and mouse cells[25, 26].

Expression of markers associated with pluripotency in VPA_AFS cells

We used immunofluorescence-based staining to detect the expression of pluripotency-associated proteins. We confirmed the flow cytometry results (**Figure 1a**) showing that endogenous OCT4 and NANOG proteins were expressed homogeneously in VPA_AFS cells (**Figure 4a**). Contrary to AFS cells, VPA_AFS cells also showed nuclear expression of DNA (cytosine-5-)-methyltransferase 3 beta (DNMT3B), ZFP42 (REX1), Oestrogen-related receptor beta (ESRRB) (which is known to interact with OCT4A to positively regulate NANOG expression[27]), LIN28A (an RNA-binding protein highly expressed in mammalian ESCs[28]), and NODAL (which signalling controls NANOG expression and functions to maintain pluripotency in human iPS cells[29] in most cells) (**Figure 4a**). Interestingly, ESRRB was expressed in VPA_AFS cells, with some, but not all, cells also expressing NODAL, suggesting that VPA_AFS cells share features of both mouse ground and human primed state of pluripotency. In contrast to hES cells, but similar to epiblast stem (EpiS) cells, VPA_AFS cells had a high cloning efficiency and survived well when dissociated as single cells, which questions their developmental origin. As expected LIN28A was localized primarily to the cytoplasm in hES cells and absent in AFS cells whereas in VPA_AFS cells, we unexpectedly observed localization of LIN28A in the nucleus, outside the nucleoli. It has been reported that in hES cells, the RNA-binding protein musashi 1 (MSI1) enhances the localization of LIN28A to the nucleus outside the nucleoli to regulate miRNA biogenesis[30], suggesting that VPA treatment may influence miRNA biogenesis.

VPA_AFS cells showed epigenetic modifications at histone 3 and 4

Modification of lysines on the tails of histones H3 and H4 plays an important role in the regulation of chromatin organisation and transcription[31], and histone acetylation contributes to the maintenance of a pluripotent state, thereby improving the accessibility of DNA to transcriptional machinery required for transcription initiation[32]. Here, we show that compared to AFS cells, VPA treatment induced acetylation at three histone H3 lysine residues, i.e. H3K9 (2.3; 2.4 and 2.3 time), K18 (1.3, 1.2 and1.3 time) and K56 (1.7, 1.9 and 1.8 time) (**Figure 4b**). These histone modifications are associated with the pluripotent state, i.e. acetylated histone H3K56 controls transcriptional and translational processes by promoting pluripotency in ESCs[33], whilst H3K18 acetylation is enriched at the promoters of *OCT4, NANOG, SOX2* and *KLF4*[32], and H3K9 acetylation predict cell self-renewal[34, 35] and reprogramming capacity[36, 37]. VPA_AFS cells also showed a slight 0.96 reduction in H4K16ac marks, which decrease promotes cellular longevity[38], (**Figure 4b**). Finally, we observed a decrease (1.4; 1.2 and 1.2 time) in the trimethylation of lysine 20 of H4, H4K20(3Me) (**Figure 4b**), which knockdown has been reported to increase the fraction of cells in S phase[39-40].

The effects of VPA treatment depended on endogeneous OCT4A activation

OCT4A, which was not expressed in AFS cells (**Figure 4a**), was expressed in VPA_AFS cells (**Figure 1a** and **Figure 4a**). To determine whether VPA directly activated OCT4A expression, we silenced endogenous OCT4 gene expression in AFS

cells and treated the cells with VPA (OCT4-shRNA VPA_AFS cells) (**Figure 5a**). We observed that VPA treatment failed to induce the expression of TRA-1-60, DNMT3B, LIN28A, NANOG, NODAL, NR6A1 and REX1, as visualised by immunofluorescence using the same exposure time (**Figure 4a and Figure 5a**), although ESRRB remained expressed (**Figure 4a**). To understand whether the absence of protein resulted from impeded translation or transcription, we assessed gene expression in (1) AFS cells, (2) VPA_AFS cells, (3) OCT4- shRNA VPA_AFS cells, (4) VPA_AFS cells following osteogenic differentiation and (5) hESCs (3 samples for each AFS-derived group) (**Figure 5b**). The results confirmed that silencing OCT4A inhibited VPA from inducing the transcriptional up-regulation of *PODXL*, *ZFP42*, *DNMT3B*, *NR6A1*, *NANOG*, *LIN28A* and *BMI1*. These data highlight OCT4A reactivation as the bottlneck of VPA-induced modification of AFS cell identity towards an earlier state of cell fate potency.

Single cell transcriptionanl profiling: homogenous expression of 14 pluripotency-associated genes in VPA_AFS cells.

We next investigated the heterogeneity of the VPA_AFS cell population using the Fluidigm microfluidics system platform[41]. This approach enabled us to simultaneously determine the expression level of 26 genes involved in pluripotency and of 10 lineage-specific genes at the single-cell level in a total of 132 individual VPA_AFS cells from three different healthy donors and in hES cells (H1) (**Figure 6a, Figure 7, Figure 8, Supplementary Figure 2, 3 and 4).** The output of the runs is a 48x48 matrix of cycle threshold (Ct) values. All three samples showed similar gene expression patterns, as indicated by the similarity of the data among the three samples tested, indicating little

effect of the genotype. In all three samples, we determined that the VPA_AFS cell population was characterised by the homogeneous expression of *OCT4*, *KLF4*, *SOX2*, *c-MYC*, *NANOG* and *LIN28A*, *TDGF1*, *NR6A1*, *DNMT3B*, *ZFP42*, *PODXL, SALL4*, *LEFTY1,* and *LEFTY2* (**Figure 6a**), which are not expressed in AFS cells (**Figure 5b**). The co-expression of *TRA-1-60*, *DNMT3B* and *REX1* has been reported to distinguish human fully reprogrammed iPSCs from partially reprogrammed cells[41]. The reactivation of *NR6A1* has been reported to distinguish pluripotent iPS cells from incompletely reprogrammed cells, and absence of expression of *NR6A1* in iPSCs results in maintenance of residual pluripotency gene expression during differentiation and improper differentiation *in vitro* and *in vivo*[42]. These results, combined with data obtained on protein expression, identify a transcriptional state for VPA_AFS cells and confirm the homogeneity of the VPA_AFS cell population. We noted that KLF4, which is already expressed in AFS cells (expression level is about 1% of that of hES cells), reached the same level as hES cells. However, we observed that the levels of expression However, the other markers were lower in VPA_AFS cells than in hES~~Cs~~ cells (**Figure 6a**). To explore this, we next used quantitative RT-PCR to compare the levels of expression of the core circuitry of pluripotency (OCT4, SOX2 and NANOG) in VPA_AFS cells to hES cells, partially reprogrammed iPS cells (14 days of reprogramming) and *bona fide* reprogrammed iPS cells (21 days of reprogramming) derived from AFS cells (**Figure 6b**). We show that expression of OCT4, SOX2 and NANOG remained lower in bona fide iPS cells than in hES cells, and that VPA_AFS cells are equivalent to iPS cells between 14 and 21 days of reprogramming (**Figure 6b**).

Single cell transcriptionanl profiling: heterogenous expression of 12 pluripotency-associated genes in VPA_AFS cells.

Other pluripotency-associated genes showed bimodal expression in VPA_AFS cells, with a distinct sub-goup of cells expressing the gene (Ct value <30) and a second sub-group showing weak or negligeable expression (Ct value >30). These markers included (1) the cyclin dependent kinase inhibition 1A and 2A *CDKN1A* and *CDKN2A*, (2) *KLF5*, (3) NODAL, (4) undifferentiated embryonic cell transcription factor 1 UTF1, (5) GDF3, (6) forkhead box protein 3 FOXD3, and (7) telomerase reverse transcriptase TERT (**Figure 7**).

However, developmental pluripotency associated 2 and 5 (*DPPA2* and *DPPA5*), Krüppel-like Factor 2 (*KLF2)* and fibroblast growth factor 4 (*FGF4*), were not expressed in VPA_AFS cells (**Figure 7**).

As *GDF3* and *TDGF1* are expressed in hESCs that are found at the top of the pluripotency gene expression hierarchy[43], we quantified the percentage of VPA_AFS cells co-expressing both genes. We found that 67% VPA_AFS cells co-expressed *GDF3* and *UTF1* (defined by a Ct value <35), with a subset of 30% cells showing higher levels of expression (Ct value < 25) for both genes (**Figure 7**). To explore this, we next investigated the molecular profile of the sub-population of cells expressing the naïve pluripotency profile, i.e. GDF3+ UTF1+ (GU+) cells, and compared it to the GDF-UTF- (GU-) cells for the 24 genes studied. Results showed that GU+ cells were not the cells expressing the heterogeneous cluster of pluripotency associated markers. However, GU+ cells expressed NODAL at a higher level (26.2±1.1 vs. 31.5±1.3, mean±std, P<0.01;) albeit still showing heterogeneity of the population (**Supplementary Figure 3a**). Performing the same transcriptome analysis on

FOXD3+ cells revealed that FOXD3+ cells do not differ from FOXD3- cells for GDF3, NODAL, TERT, KLF2, but interestingly FOXD3+ cells showed higher levels of transcripts for the pluripotency markers FGF4 (36.6±0.8 vs. 38.2±0.3, P<0.01), UTF1 (27.6±1.1 vs. 33.1±1.1, P<0.01), CDKN1A (25.6±1.2 vs. 29.8±1.2, P<0.05), CDKN2A (34.3±0.8 vs. 37.6±0.4, P<0.01), KLF5 (29.9±0.9 vs. 34.5±0.7, P<0.01), DPPA5 (33.5±0.5 vs. 36.0±0.4, P<0.01), and DPPA2 (32.3±0.5 vs. 34.9±0.4, P<0.01) (**Supplementary Figure 3b**), indicating that FOXD3+ cells, which represent 47% of the whole VPA_AFS cell population correspond to the highest expressing cells of the heterogeneous cluster of pluripotency associated transcripts.

Principle component analysis reveals the hierarchical organisation of VPA_AFS cells

Principle component analysis of the data[41] for the pluripotency-associated genes studied (**Figure 8**) revealed a group of 8 core pluripotency genes (*OCT4, KLF4, DNMT3B, SALL4, ZFP42, NR6A1, PODXL* and *SOX2*) whose expression accounted for 68% of the observed variance between VPA_AFSC cells and AFS cells. A second group of 18 genes (*LEFTY1, LEFTY2, NODAL, NANOG, TDGF1, GDF3, UTF1, TERT, DPPA2, DPPA5, CDKN1A, CDKN2A, KLF2, KLF5, FOXD3, LIN28A, c-MYC and KLF5*) explained 41% of the variance within the population.

VPA_AFS cells showed low level of expression for HLA-A, HLA-B, and HLA-C, and for markers of specific lineages (NESTIN, MAP2, T, MSX1, SOX17, GATA4 and PAX6), and expression levels were not higher that those found in hES cells, confirming that VPA_AFS cells were in a pluripotent state (**Supplementary Figure 4**).

VPA-mediated *OCT4* promoter activation occured independently of GSK3β or P13K/AKT/mTOR signaling

VPA has previously show to enhance *OCT4* promoter activity through activation of the P13K/AKT/mTOR signalling pathway activated nuclear receptors in mouse myogenic cells[57-58]. Therefore, to gain mechanistic insight into the process of VPA reprogramming, we examined whether the same mechanisms was operating in VPA-AFS cells. However, treatment of AFS cells with 1mM VPA for 2 or 24 hours did not affect the levels of phospho-AKT or phospho-mTOR (**Supplementary Figure 5a**), indicating that activation of the P13K/AKT/mTOR signalling pathway is not required for VPA to mediate OCT4 activation and revert human AFS cells to pluripotency.

VPA has pleiotropic effects which involve various pathways and multiple molecular targets such as glycogen synthase kinase 3 (GSK3β) [58]. Here, we show that VPA treatment induced GSK3β inhibition in AFS cells, which could be recapitulated by treating AFS cells with the GSK3β inhibitor CHIR99021 (**Supplementary Figure 5b**). However, treatment of AFS cells with CHIR99021 alone failed to revert the cells to pluripotency, indicating that the primary target of VPA in AFS cells is not GSK3β (**Supplementary Figure 5c**).

DISCUSSION

Here, we established a correlation between the molecular regulation of the pluripotent state in human amniocytes cultured in hESC conditions supplemented with VPA, and a description based on chromatin modifications, metabolism, cell cyle and gene expression to understand the molecular quality behind the behaviour of pluripotency.

AFS cells, which multipotent differentiation ability is routinely maintained in standard MSC cultured conditions, were adapted to feeder-free hESC culture conditions before being treated with the histone deacetylase inhibitor VPA for 5-10 days, after which VPA_AFS cells were subsequently expanded for up to 30 days in feeder-free hESC conditions. Short-term treatment with VPA reactivated the expression of endogenous *OCT4A* (along with its downstream targets), and maintained its expression level for as long as the cells were cultured in conditions maintaining the undifferentiated state of pluripotent cells. Contrary to AFS cells, VPA_AFS cells expressed *TRA-1-60* and maintained its expression long-term. In addition to *OCT4A* and *TRA-1-60*, single cell analysis and immunostaining revealed that VPA_AFS cells homogeneously expressed other pluripotency-associated genes, including *DNMT3B, REX1, NANOG, ESSRB, LIN28A, KLF4, CMYC, SOX2, NR6A1, TDGF1 and SALL4*, albeit the levels of expression found in VPA_AFS cells were lower than those observed for hESCs, explaining the results obtained on whole population transcriptome analysis, which established only a R=0.84 correlation between VPA_AFS cells and hESCs.

These results indicate that the chromatin conformation of AFS cells is permissive to chemically-induced regulation of gene expression, and that the level of *OCT4A* expression reached in VPA_AFS cells was sufficient to confer the ability of the cells to form well-differentiated teratomas *in vivo*, and to differentiate into endoderm and ectoderm-derived lineages *in vitro*.

Although VPA_AFS cells fulfilled several functional, molecular, epigenetic and metabolic characteristics that have recently been described in De Los Angeles et al.[44] as criteria of pluripotency, it is important to note that VPA_AFS cells were close, but different form hESCs. For example, only a subset of VPA_AFS cells expressed the pluripotency-associated genes *NODAL*, *TERT*, *UTF1* and *GDF3*, with only 30% of the cells co-expressing *UTF1* and *GDF3*. Interestingly, cells expressing FOXD3 showed higher transcript levels for other markers, such as CDKN1A, CDKN2A, FGF4, UTF1, KLF5, DPPA5 and DPPA2, suggesting they have reached a more advanced stage reprogramming, and it would be interesting to investigate the stability of these cells over longer period of culture. In mouse embryonic fibroblasts, an alternative class of pluripotent cells independent of standard definitions of iPS state, referred as fuzzy cells, were recently characterised, indicating that pluripotent cells can exist as different and unique states that are alternative to hESCs[45-48] The molecular events underlying functional pluripotency are not completely understood, and data from mouse and human studies indicate that pluripotency can be regained functionally without the cells reverting their cellular identity to hESCs.

We also demonstrated here that *OCT4A* was indispensible for VPA to modify the cellular identity of AFS cells. Although *OCT4* has previously been identified as the bottleneck for cellular reprogramming[49], the chemical replacement of OCT4 has yet only been achieved in mouse embryonic fibroblasts (MEFs) with a cocktail of seven small-molecule compounds[50, 51], or with the use of BrdU (bromodeoxyuridine)[52]. Our data indicate that AFS cells can be used as a model of human cells to study the chemical modulation of the pluripotency network via activation of endogenous *OCT4A*, allowing to correlate cell functionality with molecular profiling.

The mechanisms by which VPA reactivated endogenous *OCT4A* expression in AFS

cells remain speculative. VPA has pleiotropic effects on cell function, either promoting differentiation *in vitro*, facilitating the process of cellular reprogramming to pluripotency[2, 19, 53], suppressing reprogramming-induced senescence in human iPS cells[54], inhibiting autophagy via modulation of the mTORC1 signaling pathway[55], and promoting cell cycle progression and glycolysis[56]. Interestingly, VPA also enhances *OCT4* promoter activity through the activation of the P13K/Akt/mTOR signaling pathway in mouse myogenic cells[57, 58]. It has also been established that mTOR complex 1 (mTORC1) signaling regulates histone H3K acetylation on lysine-56[59-61] to promote nucleosome disassembly at promoter regions of Oct4[34]. We found that in AFS cells, VPA did not activate OCT4 promoter through the P13K/Akt/mTOR signaling pathway or GSK3β inhibition. However, the increase in acetylation of H3K9 and H3K56 marks observed in VPA_AFS cells suggest that activation of endogenous *OCT4A* might have been mediated by histone H3K56 acetylation. Elucidating the mechanisms by which VPA promoted endogenous OCT4 activity in human AFS cells provides a platform to study other small compounds which could act synergistically with VPA, paving the way for the development of chemical reprogramming of human adult somatic cells[62].

METHODS

Cell culture. Human amniocytes, i.e. amniotic fluid stem (AFS) cells, were isolated after informed consent from the amniotic fluid at 12 weeks of gestation (normal pregnancy), which was obtained under ultrasound guidance and according to the ethical approval given by the Research Ethics Committees of Hammersmith & Queen

Charlotte's Hospitals (08/H0714/87) in compliance with national guidelines (Polkinghorne) for the collection of fetal tissue for research. The AFS cells from three individuals with normal karyotype (sample 1, 2 and 3) were selected for c-KIT expression and expanded (10^4 cells/cm^2) on plastic culture dishes without feeders in Dulbecco's modified Eagle's medium (DMEM-HG) (Invitrogen) supplemented with 10% fetal bovine serum (Biosera), 2 mmol/l L-glutamine, 50 IU/ml penicillin and 50 mg/ml streptomycin (Gibco-BRL), at 37□C in a 5% CO_2 incubator. The cells were subsequently transferred onto Matrigel-coated plates (Becton Dickinson) in NutriStem XF/FF (Stemgent) for 2-5 days, after which valproic acid (VPA, 1 mM; Sigma-Aldrich) or CHIR99021 (10 μM, Stemgent) was added to the medium for a period of 5 days, after which the cells were subsequently cultured in NutriStem alone without VPA (VPA_AFS cells)[13]. NutriStem medium was replaced every 24 h. Human ES cell line H1 (WiCell Research Institute), was cultured in feeder-free conditions on Matrigel-coated plates in mTeSR (Stem Cell Technologies). NTERA2 cells (ATCC) were cultured in DMEM supplemented with 10% FBS). Microdissection passaging techniques were combined with type IV collagenase (1 mg/ml, Invitrogen) or dispase (1.5 mg/ml, Invitrogen) treatment to split cells at a ratio of 1:3. For comparative analysis to partially reprogrammed and *bone fide* iPS cells, AFS cells were reprogrammed using an episomal mixture (Invitrogen kit #A15960) over 25 days.

Colony formation in soft agar. Anchorage-independent growth was determined by suspending VPA_AFS cells and NTERA2 cells (5 x 10^3 cells) in DMEM containing 10% FBS and 0.3% of low melting agarose (Gibco BRL). The cells were plated in 12-well plates over a layer of solidified DMEM containing 10% FBS and 0.6% agarose. The medium was replaced every 3 days. Colonies were photographed after 3 weeks.

~~**Transfection**~~ **Transduction with OCT4-GFP and NANOG-GFP**. We used OCT4-GFP lentivirus and NANOG-GFP lentivirus (Cellomics Inc) in which the GFP reporter gene is expressed from the OCT4 and NANOG promoter that is active when cells are in an undifferentiated state. If the OCT4 or NANOG promoter is gradually inactivated, the GFP reporter is down-regulated. For transduction with the lentivirus, AFS cells were plated in six-well plates with 2 ml D10 culture medium and then placed back in the CO_2 incubator for 18 h prior to transduction. Aliquots of lentiviral stock were mixed with transduction medium (10 ug/ml polybrene in 2 ml growth medium). The cells were removed from the incubator, and the culture medium was aspirated and replaced with transduction medium containing the virus. The cultures were centrifuged at 1200 x g for 60 min at room temperature to increase infection efficiency. The plates were incubated at 37°C for 10 h in the CO_2 incubator. The virus-containing transduction medium was then discarded and replaced it with fresh growth medium. The cells were left to incubate for 24–48 h to enable the accumulation of the expressed protein in the target cells, after which the cells were selected using puromycin.

OCT4 gene silencing. *OCT4* was silenced in AFS cells using OCT4-short hairpin (sh)RNA (h) lentiviral particles (sc-36123, Insight Biotechnologies), which are provided as transduction-ready viral particles for gene silencing, following the manufacturer's instructions. After transduction, AFS cells expressing the *OCT4*-shRNA were selected using puromycin.

Flow cytometry and confocal immunostaining. The antibodies used for flow cytometry and immuno-staining are listed in Supplementary Table 1. The OCT4

antibody (sc-5279, Santa Cruz) is a mouse monoclonal IgG raised against amino acids 1-134 of OCT4 of human origin, and does not cross–react with OCT4 isoform B. For flow cytometry, the cells were detached and dissociated into single cells using dispase (Sigma-Aldrich), and resuspended in FACS buffer (PBS, 1% Bovine Serum Albumin; 5 x 10^5 cells/100 ul FACS-buffer). For cell-surface staining, the AFS cells and VPA_AFS cells were replated as single cells in chamber slides to assess heterogeneity of expression and cellular localisation of antigens. The VPA-AFS OCT4-shRNA cells were directly stained on cover slips placed in the cell culture dishes. The cells were stained with antibodies for 1 h at 4□C. For intracellular FACS staining, the cells were washed once in FACS buffer, fixed for 10 min in 0.01% PFA, washed twice with PBS, resuspended in permeabilisation buffer (PBS, 1% Triton) and stained as above. All samples were analysed via FACScalibur flow cytometry (Becton Dickinson) and analysed using CellQuest software. Negative controls were IgG or IgM primary antibody-specific isotypes.

For confocal immuno-staining, the cells were fixed and stained as previously described[7]. Fluorescence confocal laser scanning microscopy images were collected on a Leica TCS SP5 (X1000 PL APO oil objective) and transferred to Adobe Photoshop (Adobe Systems). Secondary antibodies were donkey anti-mouse and anti-rabbit IgG (Jackson ImmunoResearch Laboratories). hESC cells (H1) served as positive controls.

Quantitative RT-PCR. Total RNA was extracted using the RNeasy Mini RNA kit (Qiagen) and cDNA was synthesised using Pd(N)6 random hexamers (Amersham Pharmacia Biotech) and 1 ml of 200U M-MLV Reverse Transcriptase in the presence of dNTPs (Promega), according to the manufacturer's instructions. The generated

cDNA was amplified using the ABI StepOne Sequence Detector system (Applied Biosystems) and TaqMan Assay probes, as listed in Supplementary Table 2 (Thermo Fisher Scientific). Samples were normalised against the internal control (18S).

Single-cell quantitative RT-PCR. VPA_AFS cells were dissociated into single cells using dispase, resuspended in FACS buffer supplemented with 2% FBS (Biosera) and sorted into 96-well 0.2 ml PCR plates containing 5 µl of 2x CellsDirect Reaction Mix (Invitrogen) and 0.1 µl SUPERase-in (Ambion). Reverse transcription and specific transcript amplification were performed using SuperScript III Reverse Transcriptase / Platinum Taq Mix (Invitrogen) on the thermocycler as previously described[45]. The amplified cDNA was then loaded into Biomark 48.48 Dynamic Array chips using the Nanoflex IFC Controler (Fluidigm). We then used a microfluidic platform to conduct single cell qPCR in nanolitre reaction volumes using the Biomark machine. Threshold cycle (Ct), as a measurement of relative fluorescence intensity, was extracted by the Fluidigm Real-Time PCR Analysis software. The endogenous control gene was 18S.

Carbon dioxide production: CO_2 production was used as a marker of mitochondrial oxidative metabolism. The cells were cultured in 6-well plates at a density of 10^4 cells/cm^2. The culture media was then exchanged with media equivalent supplemented with [U-^{13}C] D-glucose, and each well was covered with a glass microfibre filter disc (Whatman GF/A), soaked in 3.5 M NaOH and incubated for four hours. Following this, 500 µl culture medium was transferred to a 12-ml glass tube (Exetainer, Labco, UK), and glacial acetic acid (100 µl) was injected through the septum to release $^{13}CO_2$ from bicarbonate. The filter paper was also removed and placed in a 12-ml glass tube, and CO_2 was released by the addition of glacial acetic

acid. $^{13}CO2/^{12}CO_2$ was measured in the gas phase via isotope ratio mass spectrometry. The ratio of $^{13}CO_2$ to $^{12}CO_2$ in bicarbonate is proportional to the quantity of oxidised glucose[48].

Fluorescent evaluation of ATP dynamics: One day prior to the experiment, AFS and VPA_AFS cells were seeded on 22 mm round borosilicate cover glasses and incubated at 37°C, 5% CO_2, to reach a confluence of approximatively 40% at imaging. The adherence of VPA_AFS cells to the glass surface was facilitated by coating the cover glasses with Matrigel. Cellular ATP levels were indirectly measured with the cell permeant green fluorescent Mg^{2+} indicator Magnesium Green™, which emission intensity increases without a shift in wavelength after binding to Mg^{2+}. Briefly, the cells were loaded with 5 µM Magnesium Green™ for 30 min at 37°C and 5% CO_2. After loading, the cover glasses were washed three times with recording medium, and mounted within an Attofluor metal cell chamber for microscopy (Molecular Probes™, Thermo Fisher Scientific, A-7816). Continuous live imaging was carried out using a Zeiss LSM 510 confocal laser scanning microscope (inverted configuration on an Axiovert 200 frame) equipped with a thermostated chamber (37°C) and a Fluar 40x/1.30 oil-immersion objective. A field of view with at least 10 cells was selected prior to time-series imaging of the Magnesium Green™ fluorescent signal. An argon-ion laser was used to excite the dye, and a HTF 488/543 dichroic mirror with a BP 500/550 band-pass filter was used to capture the emitted fluorescence. The settings were held constant between experiments and were chosen to reduce photobleaching of the fluorophore (laser power: 1%). The pinhole was set to produce an optical slice of ~2 µm. After the administration of oligomycin (2.5 µg/ml) to block (1) the proton flux through the F_1F_0-ATPase and (2) cytosolic ATP depletion, images were acquired every

second to follow the time-course of cytosolic ATP depletion. Regions of interest were demarcated by selecting the entire cell surface area, and the average intensity of the florescent signal was measured. Raw data were averaged in Prism 6, and the slopes of the generated curves were calculated in Microsoft Excel 10 through linear regression. Greater Mg^{2+} availability induces a faster rate of increase in Magnesium Green fluorescence intensity; thus the slope of the graph represents an indirect method to evaluate ATP depletion.

Western blotting: Protein lysates were generated using standard lysis buffer (50 mM Tris 7.5pH, 150 mM NaCl, 1 mM EDTA) containing 1% SDS with sonication to disrupt genomic DNA. Twenty-five ug β-mercaptoethanol denatured lysates were separated on a 12.5% -PAGE gel and blotted onto a Protran nitrocellulose transfer membrane (Whatman, Life Sciences). The membrane was blocked in 5% milk PBS-T (phosphate-buffered saline with 0.1% Tween-20) and immunoprobed with antibodies raised against different peptides containing different histone modifications (H3K9ac Abcam Cell Signalling 96715; H3K18ac Abcam 1191, H3K56ac epitomics 2134-1, H4K20me3 Millipore 07-463, H3 Abcam 10158 and H4 Abcam 1971 loading controls). The secondary antibodies used were goat anti-rabbit conjugated to horseradish peroxidase (HRP) (Dako) and rabbit anti-mouse-HRP (1:5000) (Dako). The experiments were performed in triplicate. Bands were quantitated via direct scanning of the western blot films with a HP Scanjet 4890 and quantified using ImageJ software. For analysis of the P13K/AKT/mTOR signalling pathway, the antibodies for phosphorylated AKT (pAKT), phosphorylated mTOR (pmTOR) and total mTOR antibodies were purchased from from Cell Signaling (#40585, #55365, #29725) and the antibody for total AKT was purchased from Abcam (#ab8932).

Statistical analysis: Statistical analysis was performed using InStat Version 3.0a statistical software (GraphPad Software, La Jolla, CA). $P < 0.05$ was significant.

Acknowledgements

We thank Professor George Q Daley and Professor Konrad Hochedlinger for helpful discussion and comments on the manuscript.

We are grateful to Professor Joseph Wu for reagents and protocols for single-cell analysis. We thank the contribution of the Confocal Microscopy (Dale Moulding) and Flow Cytometry (Ayad Eddaoudi) core facilities at the UCL Institute of Child Health. This work was supported by grants from Great Ormond Street Children's Charity, Sparks Children Medical research and Newlife Foundation and by the National Institute for Health Research Biomedical Research Centre at Great Ormond Street Hospital for Children NHS Foundation Trust and University College London. J. Adjaye acknowledges the medical faculty of Heinrich Heine University for financial support.

Author contributions

K. E. Hawkins performed AFSC culture, embryonic stem cells culture, generation and characterisation of episomal induced pluripotent stem cells, VPA-induced reprogramming to pluripotency, cell cycle analysis, flow cytometry, metabolic analysis, validation of GFP-reporters, immuno-fluorerscence, transfection, western blotting, data analysis and interpretation, preparation of figures and contribution to manuscript writing. D. Moschidou performed cell culture work, confocal microscopy, flow cytometry, transfections, gene silencing and quantitative real time RT-PCR

validations. V. Sanchez-Freire and D. Moschidou performed the single-cell real time RT-PCR and analysed the data. AM. Ranzoni and K-L. Hau performed the soft agar colony formation assay. S. Eaton performed the carbon dioxide production experiment. M. Campanella, F. Tommasini and D. Faccenda performed and analysed the fluorescent evaluation of ATP dynamics. D.Moschidou, D. Monk and A. Martin-Trujillo performed the western blotting. W. Wruck performed the analysis of the microarray data. P. De Coppi. and J. Adjaye contributed to the study design. A.J. Thrasher and P.V. Guillot designed the study and wrote the manuscript.

REFERENCES

1. Takahashi, K., et al. Induction of pluripotent stem cells from adult human fibroblasts by defined factors. Cell **131**, 861-72 (2007).
2. Huangfu, D., et al. Induction of pluripotent stem cells from primary human fibroblasts with only Oct4 and Sox2. Nat Biotechnol. **26**, 1269-75 (2008).
3. Choi, H. W., et al. Neural stem cells differentiated from iPS cells spontaneously regain pluripotency. Stem Cells **32**, 2596-04 (2014).
4. Nakagawa, M., et al. A novel efficient feeder-free culture system for the derivation of human induced pluripotent stem cells. Sci Rep. **4**, 3594 (2014).
5. Kim, J. B., et al. Direct reprogramming of human neural stem cells by OCT4. . Nature **461**, 649-03 (2009).
6. Liu, T., et al. High Efficiency of Reprogramming CD34+ Cells Derived from Human Amniotic Fluid into Induced Pluripotent Stem Cells with Oct4. Stem Cells Dev **21**, 2322-2332 (2012).
7. Guillot, P. V., et al. Human first trimester fetal mesenchymal stem cells (MSC) express pluripotency markers, grow faster and have longer telomeres compared to adult MSC. Stem Cells **25**, 646-54 (2007).
8. Moorefield, E. C., et al. Cloned, CD117 selected human amniotic fluid stem cell are capable of modulating the immune response. PLoS ONE **6**, e26535 (2011).
9. De Coppi, P., et al. Isolation of amniotic stem cell lines with potential for therapy. Nat. Biotechnol **25**, 100-06 (2007).
10. Dominici, M., et al. Minimal criteria for defining multipotent mesenchymal stromal cells. Cytotherapy **8**, 315-317 (2006).

11. Keating, A. mesenchymal stromal cells: new directions. Cell Stem Cell **10**, 709-716 (2012).

12. Moschidou, D., et al. Valproic acid confers functional pluripotency to human amniotic fluid stem cells in a transgene-free approach. Mol. Ther. **20**, 1953-67 (2012).

13. Moschidou, D., et al. Molecular signature of human amniotic fluid stem cells during fetal development. Curr Stem Cell Res Ther **8**, 73-81 (2013).

14. Moschidou, D., et al. Human mid-trimester amniotic fluid stem cells cultured under embryonic stem cell conditions with vaproi acid acquire pluripotency characteristics. Stem Cells Dev **22**, 444-58 (2013).

15. Wang, X., et al. Isoforms of OCT4 Contribute to the Confusing Diversity in Stem Cell Biology. Stem Cells **28**, 885-893 (2010).

16. Li, C., et al. Pluripotency can be rapidly and efficiently induced in human amniotic fluid-derived cells. Hum Mol Genet **18**, 4340-4349 (2009).

17. Galende, E., et al. Amniotic fluid cells are more efficiently reprogrammed to pluripotency than adult cells. Cell Reprogram **2**, 117-125 (2010).

18. Wolfrum, K., et al. The LARGE principle of cellular reprogramming: lost, acquired and retained gene expression in foreskin and amniotic fluid-derived human iPS cells. PLoS One **5**, e13703 (2010).

19. Kostrouchová, M., et al. Valproic acid, a molecular lead to multiple regulatory pathways. Folia Biologica (Praha) **53**, 37-49 (2007).

20. Diecke, S. e. a. Pushing the reset button: chemical-induced conversion of amniotic fluid stem cells into a pluripotent state. Mol Ther **10**, 1839-1841 (2012).

21. Tanabe, K., et al. Maturation, not initiation, is the major roadblock during reprogramming toward pluripotency from human fibroblasts. . Proc Natl Acad Sci U S A. **110**, 12712-9 (2013).

22. Singh, A. M., et al. The cell cycle and Myc intersect with mechanisms that regulate pluripotency and reprogramming. Cell Stem Cell **5**, 141-149 (2009).

23. Li, V. C., et al. Gap 1 phase length and mouse embryonic stem cell self-renewal. . Proc Natl Acad Sci U S A. **109**, 12550-12555 (2012).

24. Coronado, D. e. a. A short G1 phase is an intrinsic determinant of naïve embryonic stem cell pluripotency. Stem Cell Res **10**, 118-131 (2013).

25. Panopoulos, A. D., et al. The metabolome of induced pluripotent stem cells reveals metabolic changes occurring in somatic cell reprogramming. Cell Res **22**, 168-177 (2012).

26. Prigione, A., et al. The Senescence-Related Mitochondrial/Oxidative Stress Pathway is Repressed in Human Induced Pluripotent Stem Cells. Stem Cells **28**, 721-733 (2010).

27. Van Den Berg, D., et al. Estrogen-related receptor beta interacts with Oct4 to positively regulate Nanog gene expression. Mol Cell Biol. **28**, 5986-95 (2008).

28. Shy-Shang, N., et al. Lin28 enhances tissue repair by reprogramming cellular metabolism. Cell **155**, 778-92 (2013).

29. Vallier, L., et al. Signaling Pathways Controlling Pluripotency and Early Cell Fate Decisions of Human Induced Pluripotent Stem Cells. Stem Cells **27**, 2655-66 (2009).

30. Tsialokas, J., et al. LIN28: roles and regulation in development and beyond. Development **142**:2397-2404 (2015).

31. Jenuwein, T., et al. Translating the histone code. Science **293**, 1074-1080 (2001).

32. Kumar, S., et al. Chromatin remodeling of embryonic stem cells by E1A alters global histone H3 lysine 18 acetylation and loss of pluripotency. J Investig Genomics **1**, 9-20 (2014).

33. Tan, Y. Acetylated histone h3K56 interacts with Oct4 to promote mouse embryonic stem cell pluripotency. Proc Natl Acad Sci U S A. **110**, 11493-11498 (2013).

34. Krejci, J., et al. Genome-wide reduction in H3K9 acetylation during human embryonic stem cell differentiation. J Cell Physiol **9**, 677-87 (2009).

35. Meissner, A., et al. Genome-scale DNA methylation maps of pluripotent and differentiated cells. Nature **454**, 766-770 (2008).

36. Hezroni, H., et al. Pluripotency-related, valproic acid (VPA)-induced genome-wide histone H3 lysine 9 (H3K9) acetylation patterns in embryonic stem cells. J Biol Chem. **286**, 35977-88 (2011).

37. Hezroni, H., et al. H3K9 histone acetylation predicts pluripotency and reprogramming capacity of ES cells. Nucleus 2, 300-309 (2011).

38. Dang, W., et al. Histone H4 lysine 16 acetylation regulates cellular lifespan. Nature **459**, 802-807 (2009).

39. marion, R. M., et al. Suv4-20h abrogation enhances telomere elongation during reprogrmming and confers a higher tumorigenic potential to iPS cells. PLoS ONE **6**, e25680 (2011).

40. Evertts, A. G., et al. H4K20 methylation regulates quiescence and chromatin compaction. Mol Biol Cell **24**, 30225-3037 (2013).

41. Sanchez-Freire, V., et al. Microfluidic single-cell real-time PCR for comparative analysis of gene expression patterns. Nat Protoc **7**, 829-838 (2012).

42. Wang, H., et al. Epigenetic re-programming of the Germ Cell Nuclear Factor gene is required for proper differentiation of induced pluripotent cells. Stem Cells **31**, 2659-66 (2013).

43. Hough, S. R. A continuum of cell states spans pluripotency and lineage commitment in human embryonic stem cells. PLoS ONE **4**, e7708 (2009).

44. De Los Angeles, A., et al. Hallmarks of pluripotency. Nature **525**, 469-478 (2015).

45. Hussein, A. M. I., et al. Genome-wide characterisation of the routes to pluripotency. Nature **516**, 198-206 (2014).

46. Tonge, P. D., et al. Divergent reprogramming routes lead to alternative stem-cel states. Nature **516**, 192-7 (2014).

47. Clancy, J. L., et al. Small RNA changes en route to distinct cellular states of induced pluripotency. Nat Commun. **5**, 5522 (2014).

48. Lee, D. S., et al. An epigenomic roadmap to induced pluripotency reveals DNA methylation as a reprogramming modulator. Nat Commun. **5**, 5619 (2014).

49. Jerabek, S., et al. OCT4: Dynamic DNA binding pioneers stem cell pluripotency. Biochim Biophys Acta **1839**, 138-154 (2014).

50. Hou, P., et al. Pluripotent stem cells induced from mouse somatic cells by small-molecule compounds. Science **431**, 651-53 (2013).

51. Zhao, Y., et al. a XEN-like state bridges somatic cells to pluripotency during chemical reprogramming. Cell **163**, 1678-1691 (2015).

52. Long, Y., et al. Bromodeoxyuridine promotes full-chemical induction of mouse pluripotent stem cells. Cell Res **25**, 1171-1174 (2015).

53. Huangfu, D., et al. Induction of pluripotent stem cells by defined factors is greatly improved by small-molecule compounds. Nat Biotechnol. **26**, 795-7 (2008).

54. Chen, X., et al. Valproic acid enhances iPSC induction from human bone marrow-derived cells through the suppression of reprogramming-induced senescence. J Cell Physiol, Epub ahead of print (2015).

55. Jung, C. H., et al. mTOR regulation of autophagy. FEBS Lett **584**, 1287-1295 (2010).

56. Watson, A. S., et al. Autophagy limits proliferation and glycolytic metabolism in acute myeloid leukemia. Cell Death Discov **1**, 15008 (2015).

57. Teng, H. F., et al. Valproic acid enhances Oct4 promoter activity in myogenic cells. J Cell Biochem. J Cell Biochem **110**, 995-04 (2010).

58. Teng, H. F., et al. Valproic acid enhances Oct4 promoter activity through PI3K/Akt/mTOR pathway activated nuclear receptors. Mol Cell Endocrinol **383**, 147-58 (2014).

59. Williams, S. K., et al. Acetylation in the globular core of histone H3 on lysine-56 promotes chromatin disassembly during transcriptional activation. Proc Natl Acad Sci U S A. **105**, 9000-9005 (2008).

60. Chen, H., et al. The histone H3 lysine 56 acetylation pathway is regulated by target of rapamycin (TOR) signaling and functions directly in ribosomal RNA biogenesis. Nucleic Acids Res. **40**, 6534-6546 (2012).

61. Liu, Y., et al. Oncogene Ras/Phospatidylinositol 3-kinase (P13K) signaling targets histone H3 acetylation at lysine K56. J Biol Chem **287**, 1469-1480 (2012).

62. Cheng, X., et al. Identification of 2-[4-[(4-Methoxyphenyl)methoxy]-phenyl]acetonitrile and Derivatives as Potent Oct3/4 Inducers. J Med Chem **58**, 4976-4983 (2015).

FIGURE LEGENDS

Figure 1 | VPA_AFS cells are similar yet different from hES cells. (a) Flow cytometry for expression of the cell surface markers TRA-1-60, TRA-1-81, SSEA3, and for the nuclear markers NANOG and OCT4 in hES cells, AFS cells (whole population) and VPA_AFS cells (whole population). The red tracing shows the isotype control and the blue tracing shows the primary antibody. **(b)** Scatter plot (log2) of VPA_AFS cells (whole population) and two hESCs lines (H1 and H9), and heatmap of pluripotency associated genes generated via similarity measure Pearson correlation (color scaling per row/gene) using the transcriptome profiling data of the cells acquired previously using the Human Ref-8 v3.0 expression BeadChip platform (NCBI Gene expression omnibus, GSE26940).

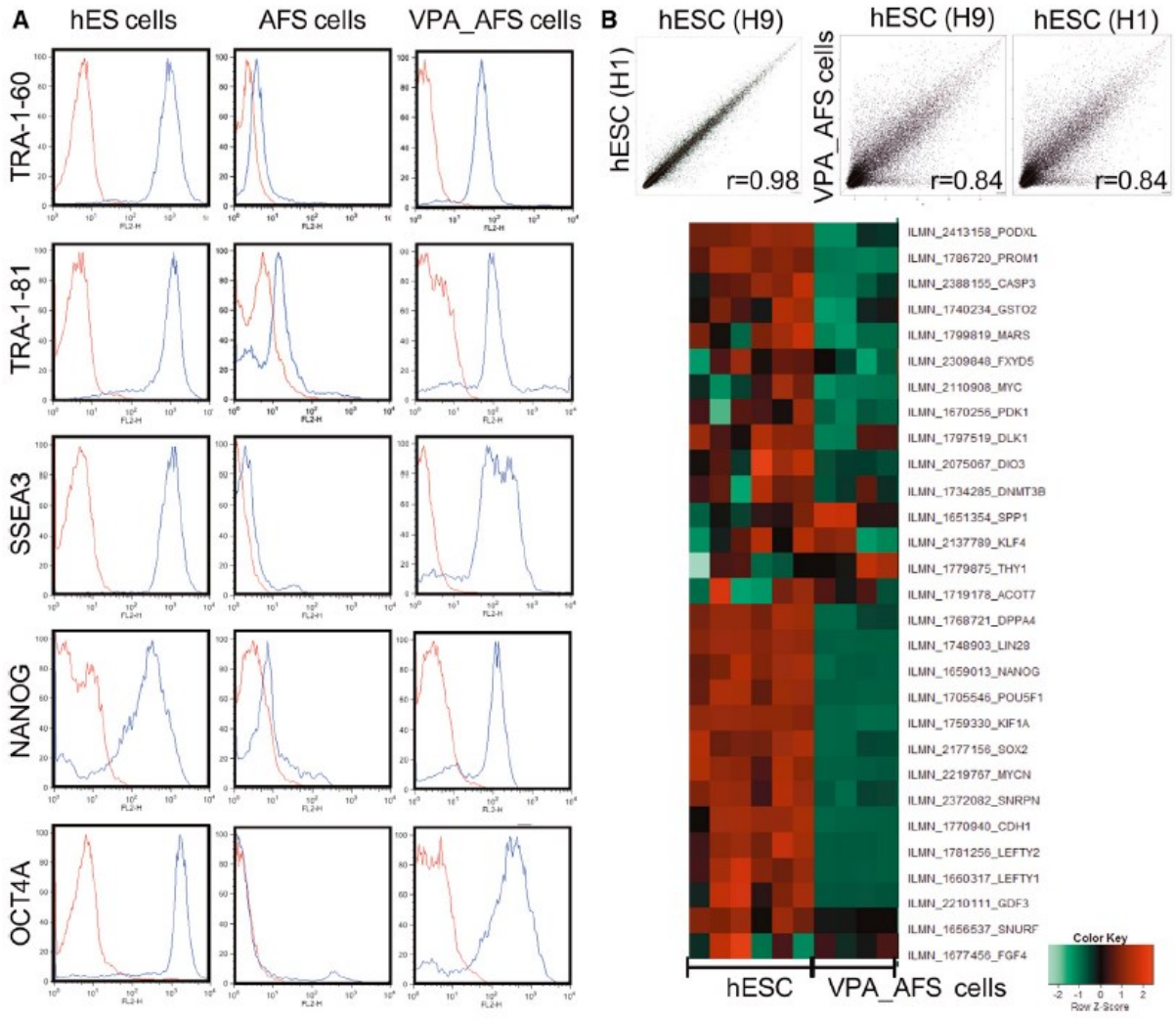

Figure 2 | Efficiency of the VPA treatment. (a) AFS cells transfected with OCT4-GFP or NANOG-GFP reporters genes were cultured on plastic culture dishes in growth medium composed of DMEM supplemented with 10% FBS before being transferred on Matrigel-coated dishes in Nutristem medium for 7 to 14 days prior to exposure to 1 mM VPA for 5 days (VPA_AFS Cells). TRA-1-60^{+} cells were subsequently single-cell sorted into four 96-well plates, and cultured for another 28 days in Nutristem (supplemented with a ROCK inhibitor to increase cloning efficiency) on Matrigel. In parallel, the whole VPA_AFS cell population was also maintained in culture for 28 days. **(b)** The number of OCT4-GFP^{+} or NANOG-GFP^{+} clones was monitored at 7, 14 and 28 days in the 96-well plates, and the GFP intensity was recorded at 7 and 28 days using an optical plate reader. **(c)** TRA-1-60 expression was assessed by flow cytometry (the red tracing shows the isotype control and the blue tracing shows the primary antibody) in the VPA_AFS cell population after 28 days in culture in Nutristem. **(d)** NANOG-GFP and OCT4-GFP immunostaining in hES cells. OCT4-GFP was validated using immunosfluorescence in hES cells using OCT4A-specific antibody.

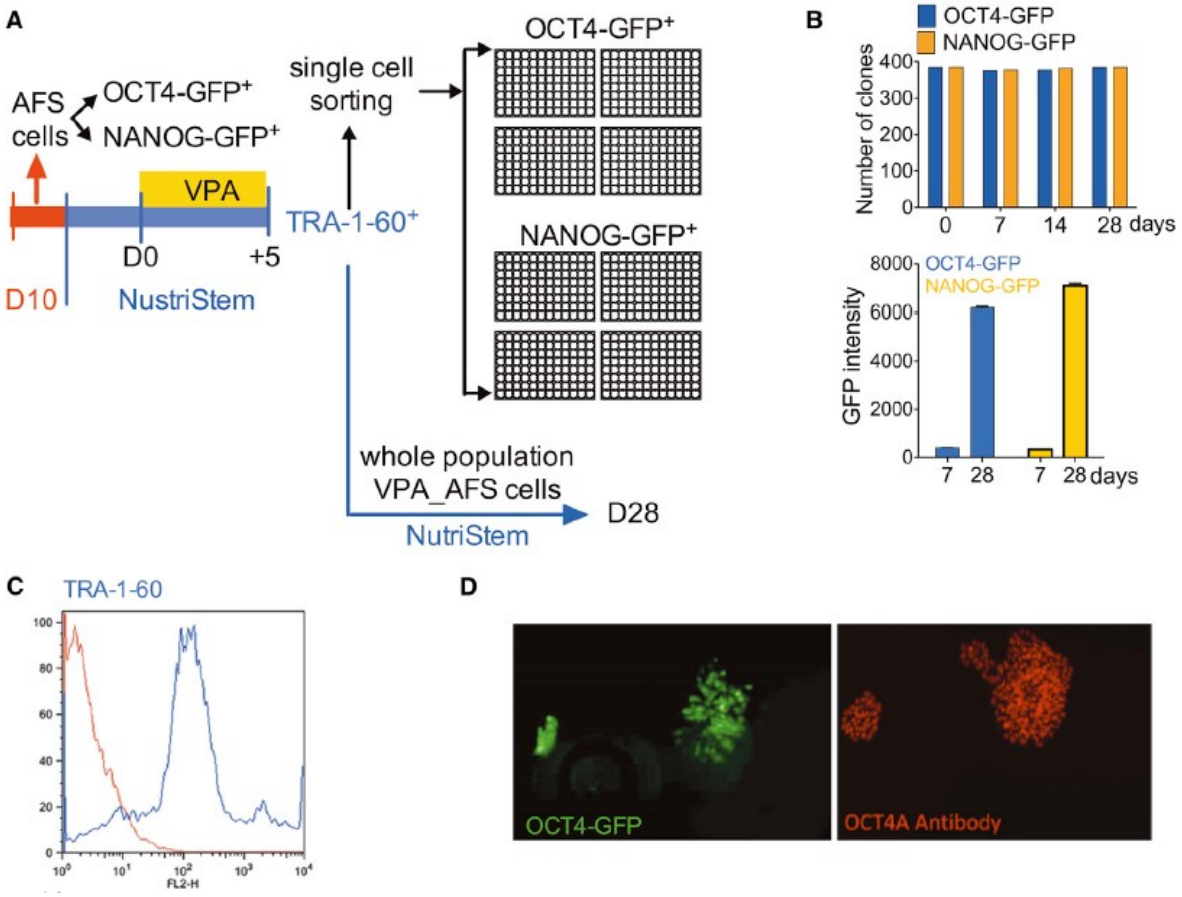

Figure 3 | Cell size, cell cycle and metabolism of AFS and VPA_AFS cells. (a) Phase contrast images of VPA_AFS cells (left panel, x40 magnification) and confocal immuno-fluorescence showing the morphology of the cells growing as compact colonies (right panel). Nuclei stained with DAPI (blue). Actin filaments stained with Alexa Fluor 594 Phalloidin (red). Scale bar 50μm. **(b)** Flow scatter and histogram showing differences in the relative size of parental AFS cells (pink) and VPA_AFS cells (blue). **(c)** Flow cytometry of AFS cells, VPA_AFS cells expanded for 28 days in NutriStem on Matrigel, and hES cells showing DNA stained with propidium iodide. G1 indicates cells with 2n cellular DNA content, S indicates cells undergoing mitosis, and G2/M indicates cells with 4n cellular DNA content. **(d)** Magnesium green fluorescence intensity staining, as a function of ATP levels, over time for parental AFS cells and VPA_AFS cells following the addition of 2.5 μg/ml OLIGO. Representative traces depicting oligomycin-induced ATP depletion for parental AFS cells and VPA_AFS cells. Cells were loaded with Mg^{2+} indicator Magnesium Green™ and AM to obtain an indirect measurement of cellular ATP levels over time. Upon the addition of oligomycin (2.5 μg/ml), a rapid increase in Magnesium Green™ emitted fluorescence is observable in AFS cells. The bar chart on the right reports the average slopes of increase in Magnesium Green™ fluorescence for AFS cells and VPA_AFS cells ($n = 3$, $p < 0.005$). **(e)** Oxidative phosphorylation studied using carbon isotope labelling of [U-^{13}C] glucose, followed by CO_2 release, isotype analysis and quantification in AFS cells, VPA_AFS cells, hES cells, and AFS cells differentiated for 2 weeks down the osteogenic lineage. *** $P<0.001$.

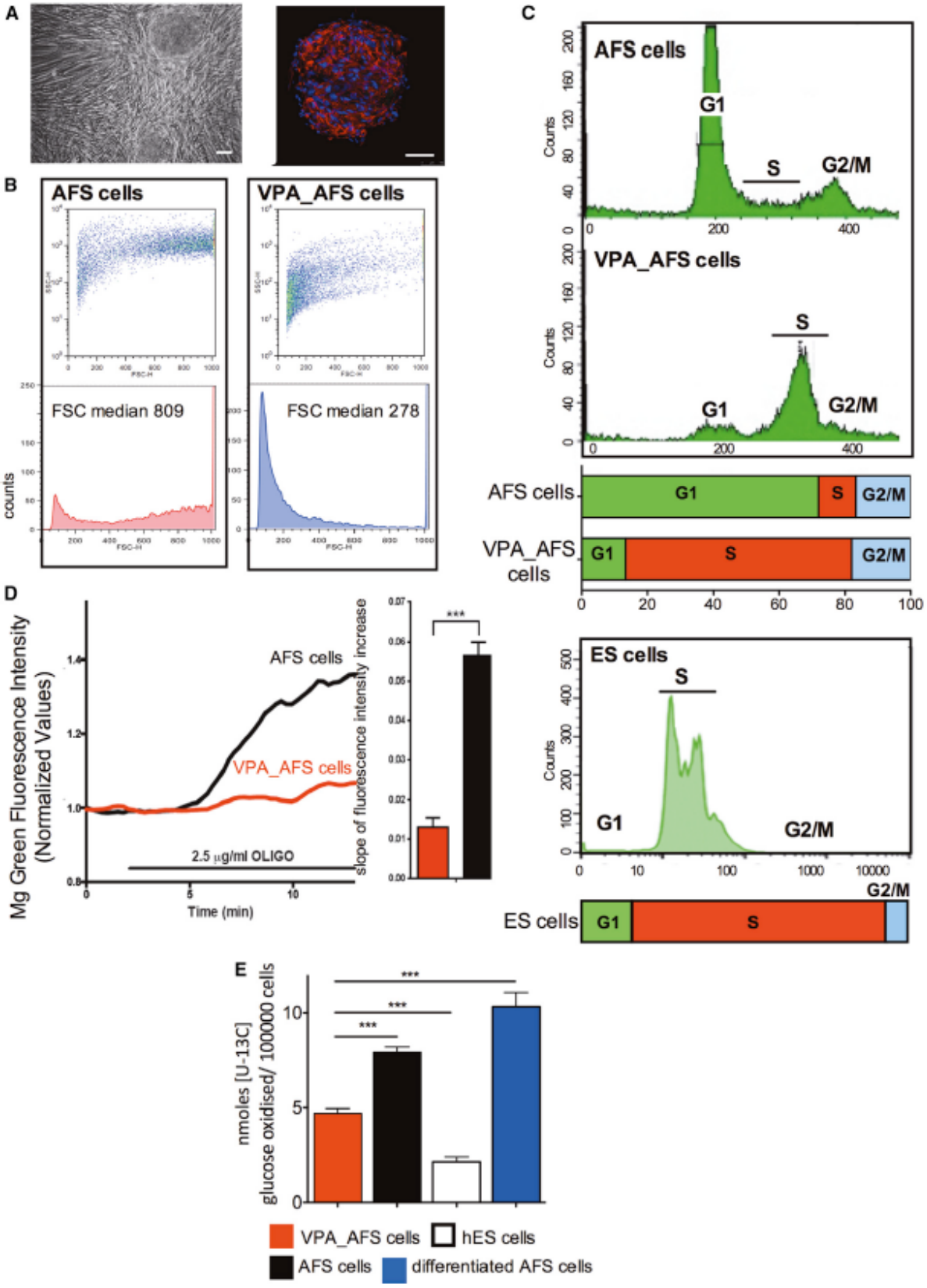
A
B
AFS cells
VPA_AFS cells
FSC median 809
FSC median 278
counts
C
AFS cells
G1
S
G2/M
Counts
VPA_AFS cells
AFS cells
VPA_AFS cells
ES cells
D
Mg Green Fluorescence Intensity (Normalized Values)
AFS cells
VPA_AFS cells
2.5 µg/ml OLIGO
Time (min)
slope of fluorescence intensity increase
***
E
nmoles [U-13C] glucose oxidised/ 100000 cells
VPA_AFS cells
hES cells
AFS cells
differentiated AFS cells

Figure 4 | VPA_AFS cells gain the expression of pluripotency markers and undergo histone modifications. (a) Confocal immuno-fluorescence showing expression of DNMT3B, REX1, OCT4A, NANOG, ESRRB, LIN28A, and NODAL stained with FITC (green) in hESCs, AFS cells, VPA_AFS cells and OCT4-shRNA cells using the same exposure time. The nuclei are stained with DAPI (blue). Actin filaments are stained with Alexa Fluor 594 Phalloidin (red). Scale bar 50μm. **(b)** Western blotting for histone modification detection in AFS cells and VPA_AFS cells. Lysates were made and western blot was performed with antibodies against acetylated and methylated lysines located on the N-terminal histone tails and compared with the total H3 and H4 loading controls.

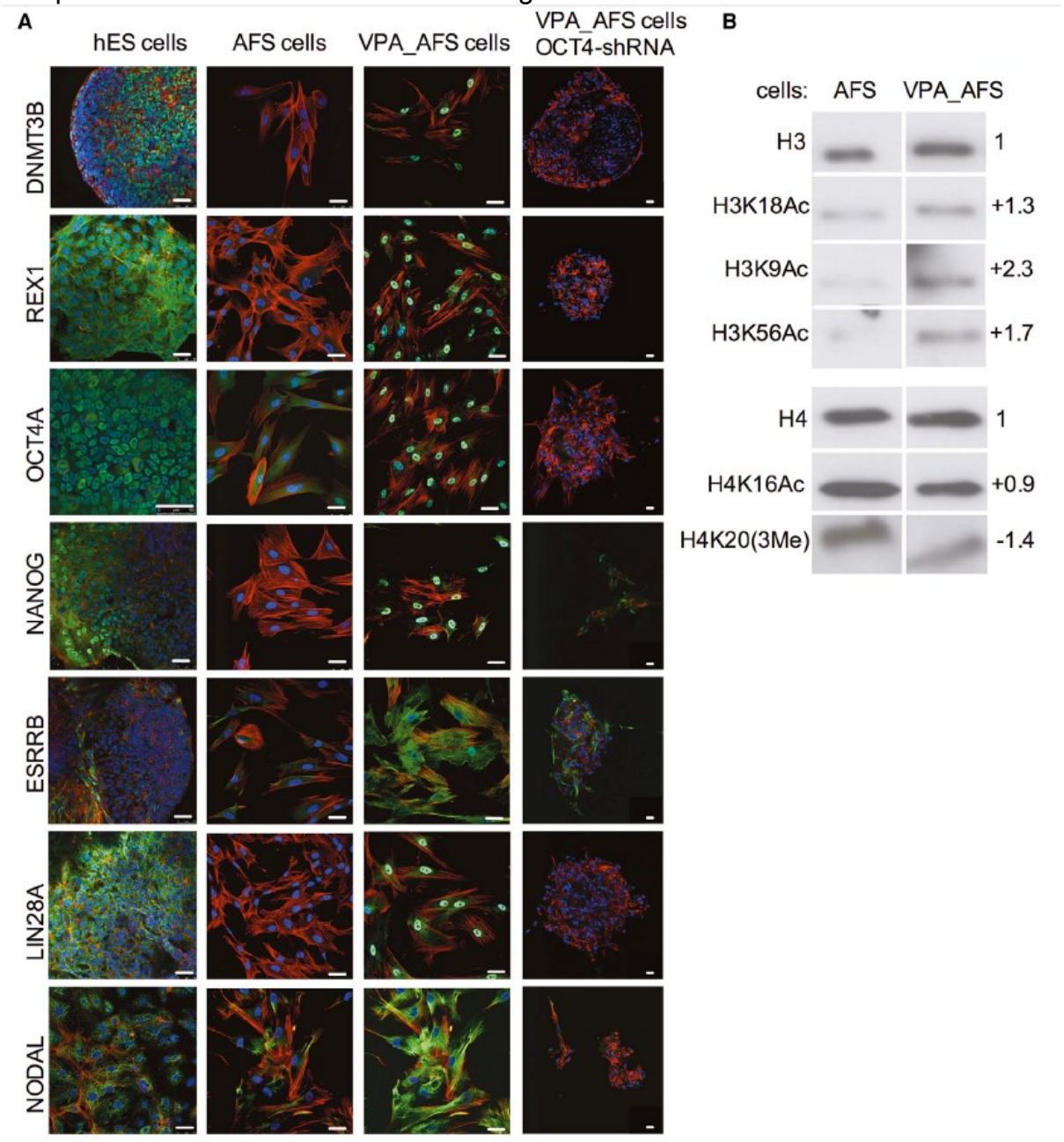

Figure 5 | Blocking OCT4A expression in AFS cells prevents VPA from inducing the up-regulation of pluripotency markers. (a) Flow cytometry showing OCT4 and TRA-1-60 expression in OCT4-shRNA VPA_AFS cells. The red tracing shows the isotype control and the blue tracing shows the primary antibody. **(b)** Quantitative RT-PCR for the housekeeping genes *18S* and *ACTIN,* and for the pluripotency markers *OCT4A, PODXL, ZFP42, DNMT3B, NR6A1, TGFB1, NANOG, LIN28A*, and *BMI-1* in AFS cells (n = 3, blue bars), VPA_AFS cells (n = 3, red bars), OCT4-shRNA VPA_AFS cells (n = 3, yellow bars), AFS cells differentiated down the osteogenic lineage (n = 3, green bars), and hESCs (n=2, black bars)., error bars are s.e.m.

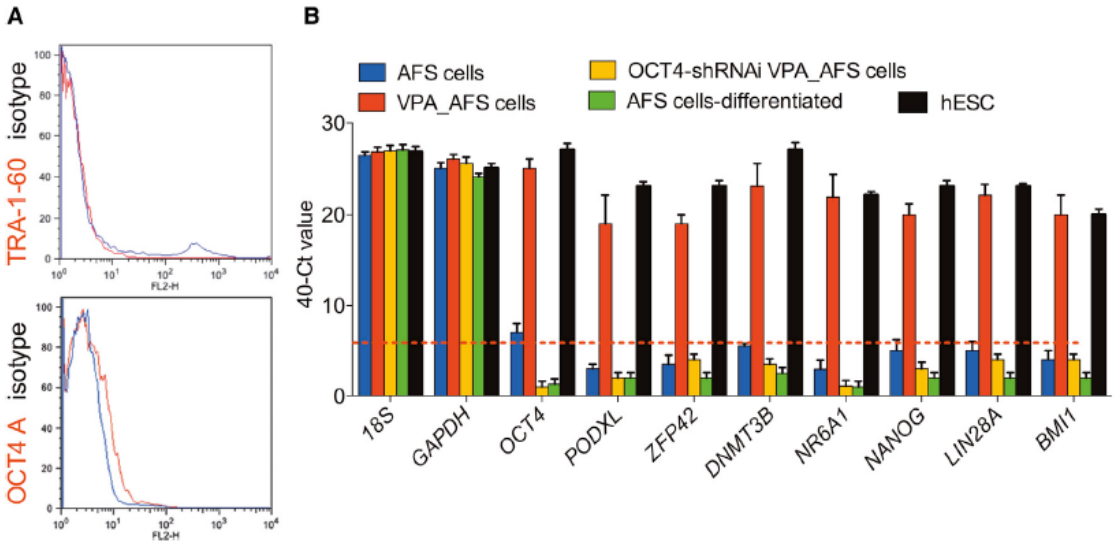

Figure 6 | Single-cell transcriptional profiling: homogenous expression of 14 pluripotency-associated genes in VPA_AFS cells. (a) Population distribution for 3 different VPA_AFS cell samples (S1, S2 and S3, 46 cells per sample) and hESCs showing homogeneity in the expression of 14 genes associated with pluripotency (*OCT4, KLF4, SOX2, CMYC, NANOG, LIN28A, TDGF1, NR6A1, DNMT3B, REX1, PODXL, SALL4*, *LEFTY2* and *LEFTY1)*. Each point represents the expression value of a single cell. The horizontal axis represents the Ct value. The red bar indicates the mean Ct value. **(b)** Quantitative real-time RT-PCR for *OCT4, SOX2* and *NANOG* in hES cells (n = 3, blue bars), iPS cells at day 14 (n = 3, red bars), day 21 (n = 3, yellow bars), fully reprogrammed iPS cells (n = 3, green bars) and VPA_AFS cells (n = 3, black bars). Housekeeping genes for normalisation were GAPDH and 18S. error bars are s.e.m

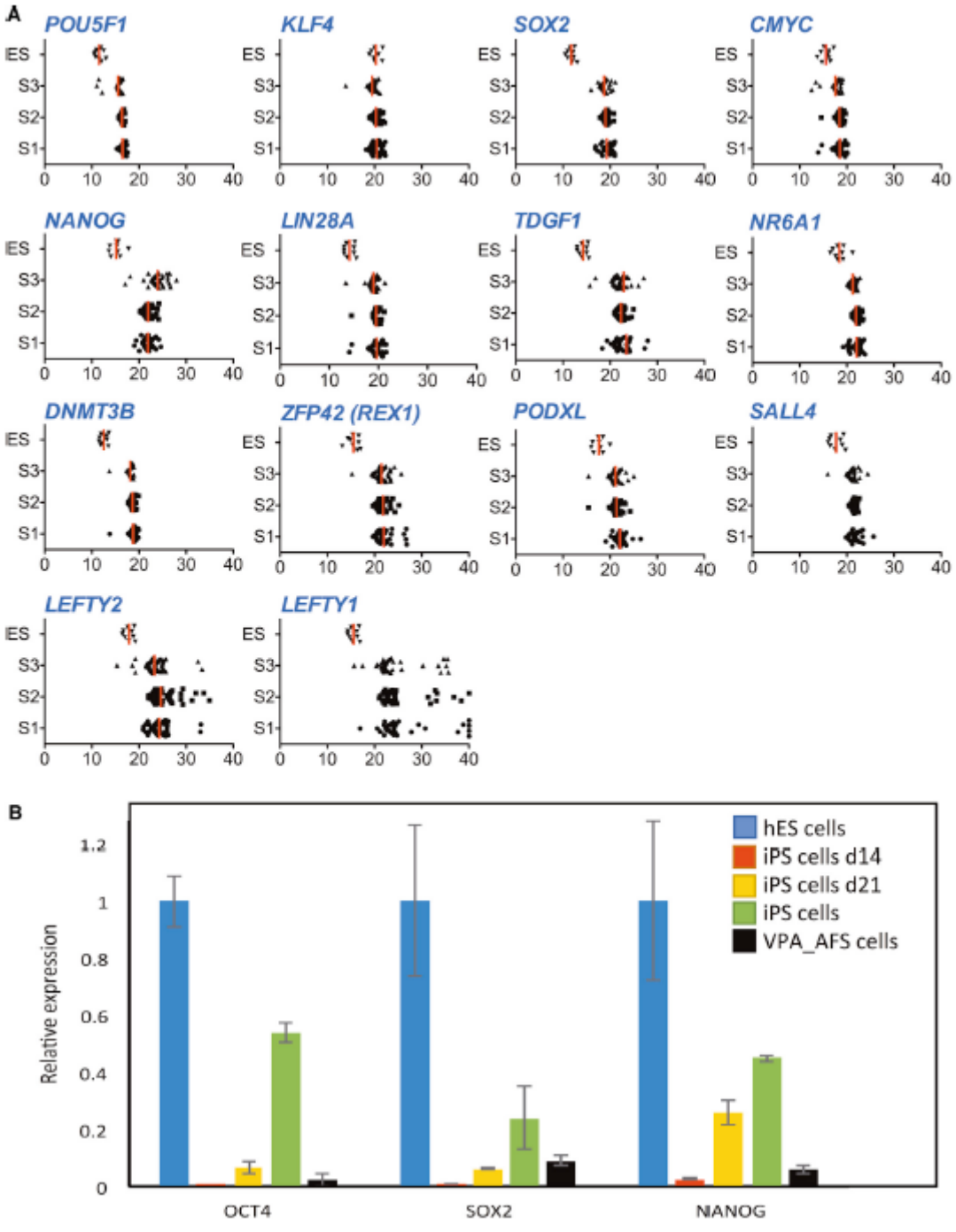

Figure 7 | Single-cell transcriptional profiling: heterogenous expression of 12 pluripotency-associated genes in VPA_AFS cells. (a) Population distribution for 3 different VPA_AFS cell samples (S1, S2 and S3, 46 cells per sample) and hESCs showing heterogeneity in the expression of 12 genes associated with pluripotency (*CDKN1A, CDKN2A, KLF5, NODAL, UTF1, GDF3, FOXD3, TERT, KLF2, DPPA2, DPPA5, and FGF4).* The red bar indicates the mean Ct value. **(c)** Distribution of Ct values for *UTF1* (horizontal axis) and *GDF3* (vertical axis) in VPA_AFS cells.

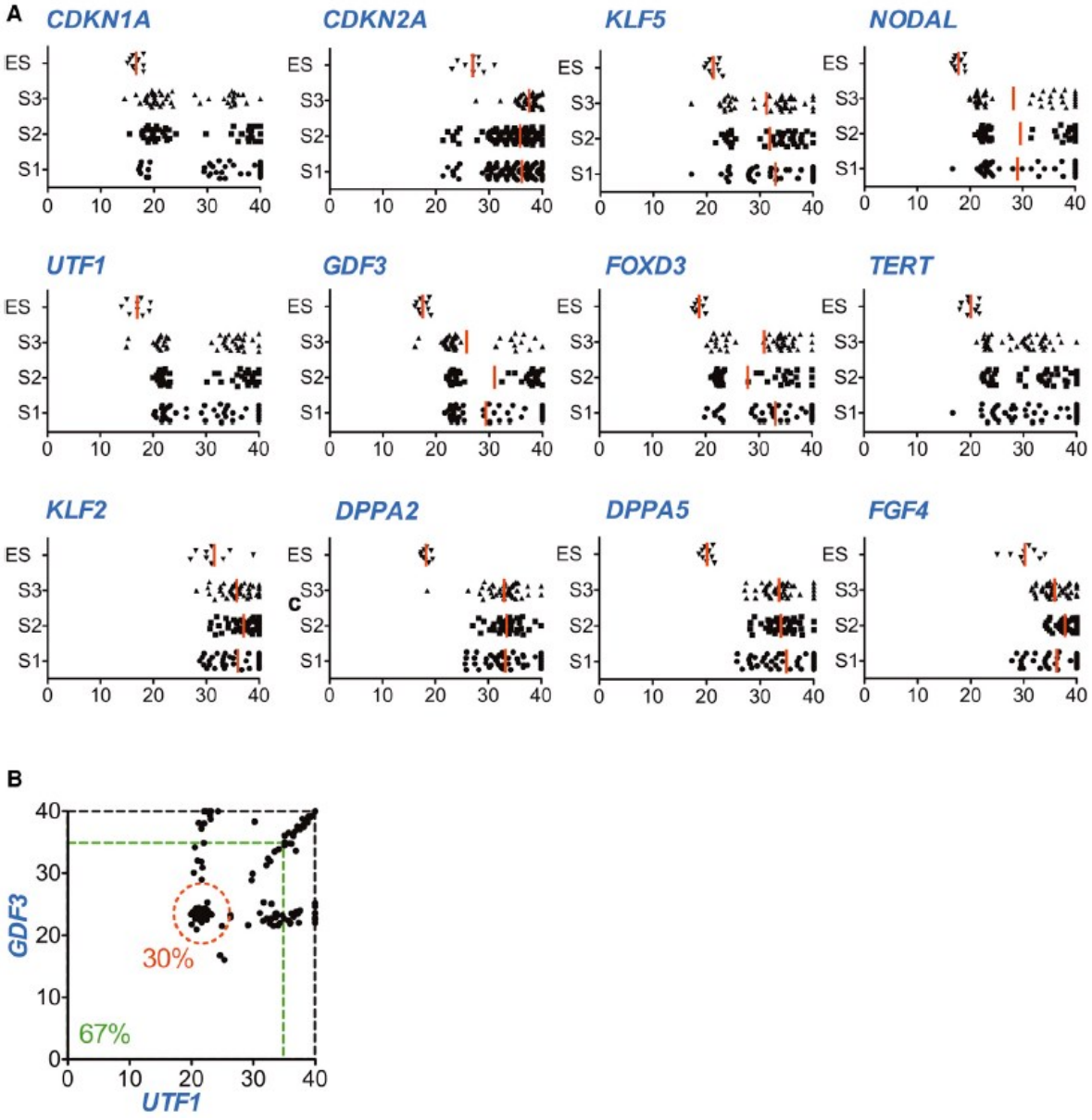

Figure 8 | Principal component analysis of VPA_AFS cells. Principal component analysis for 26 pluripotency genes in 3 samples (138 cells analysed per gene) and corresponding biplots.